Calcite Growth Kinetics: Dependence on Saturation Index, $Ca^{2+}:CO_3^{2-}$ Activity Ratio, and Surface Atomic Structure

K. K. Sand,[*,†] D. J. Tobler,[†] S. Dobberschütz,[†] K. K. Larsen,[‡] E. Makovicky,[§] M. P. Andersson,[†] M. Wolthers,[∥,⊥] and S. L. S. Stipp[†]

[†]Nano-Science Center, Department of Chemistry, [‡]Centre for Star and Planet Formation, Natural History Museum of Denmark, and [§]Department of Geography and Geology, University of Copenhagen, Copenhagen, Denmark

[∥]Department of Earth Sciences, Geochemistry, Faculty of Geosciences, Utrecht University, Utrecht, The Netherlands

[⊥]Department of Chemistry, University College London, London, United Kingdom

S *Supporting Information*

ABSTRACT: It is becoming increasingly clear that the rate of crystal growth, even at constant saturation, varies with pH, ionic strength, and solution stoichiometry. Here, we contribute to the limited data set on experimentally obtained calcite step velocities from solutions with strictly controlled parameters. We measured growth on obtuse and acute edges in solutions with five $Ca^{2+}:CO_3^{2-}$ activity ratios (r): 0.1, 1.0, 10, 25, and 50, at three saturation indices: SI = 0.6, 0.8, and 1.0. The curve describing rate as a function of r is not centered at $r = 1$, and the maximum velocity is different for each step. Obtuse steps generally grow faster in Ca^{2+}-rich solutions, i.e., $r > 1$, whereas the acute rates dominate when CO_3^{2-} is in excess, i.e., $r < 1$. We show that the local arrangement of every second carbonate at the acute steps can help explain these rate differences. To further analyze the differences in growth rates, we fitted four currently used growth models to our data set, to derive growth parameters for each type of step. Some of the models worked for some of the conditions, but none could describe the results over the full range of our experiments.
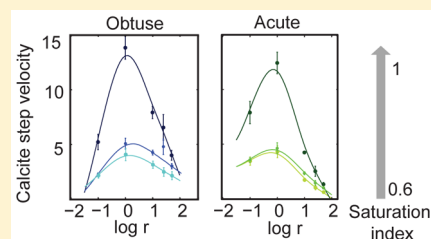
INTRODUCTION

Calcite is a common mineral in nature and industry, and it has been widely investigated because of its prominent role in geochemical, biological, geological, and industrial processes, as well as in the global carbon cycle.[1] The ability to predict growth in aqueous systems containing calcite requires data for growth rates that are dependable over a range of conditions. Several decades of research have provided a good understanding of the relationship between rates and the thermodynamic driving force for calcite growth in stoichiometric solutions, for example, refs [2–6]. However, we are not yet able to completely explain the differences in growth rate that are observed on the structurally distinct sites on calcite steps at nonstoichiometric conditions. To understand the relationship between step advance and local atomic structure, better fundamental information about the molecular surface processes and rates of reaction is needed. Such insight can be obtained by combining experimental measurements from calcite growth spirals with kinetic parameters derived from process based growth models.

Calcite ($CaCO_3$) is a rhombohedral mineral, where the most stable crystal plane formed by the structure is {10.4}. Because of its rhombohedral form, the three symmetric cleavage planes produce step edges that form acute and obtuse edges with the terraces. The bulk atomic structure results in two alternating local arrangements of atoms on the obtuse step edges and two others on the acute step edges.[7–9] Space at the obtuse step is open, whereas the acute step is more constricted. In solutions of low to intermediate calcite supersaturation (saturation index, SI ≤ 0.8), growth is dominated by advancing molecular layers that are generated at crystal defects such as edge or screw dislocations,[10–13] where the driving force for ion attachment is higher than on the surrounding surface, for example, refs [14] and [15]. In many cases, dislocation pyramids result. These consist of steps that form a continuous growth spiral. In solutions where SI > 0.8, the frequency of two-dimensional surface nucleation increases,[13] and spiral growth gives way to 2D nucleation.

Detailed investigations of growth spiral step velocity and geometry provide a window into the kinetics of calcite growth. Previous experimental studies, with and without coupled modeling, have provided insight into the molecular processes of ion attachment and detachment at the structurally distinct steps. However, comparison between these studies is challenging because the models that have been applied differ considerably in their assumptions about the mechanisms, and the data have been obtained over quite different solution conditions. Indeed, studies on step growth provided a wide range of velocities, which can be explained by the sensitivity of growth rate to solution composition. Velocity has been

reported for each step type as a function of: Ca^{2+} to CO_3^{2-} ratio, r;[14−16] saturation index, SI;[16,17] pH;[18−20] ionic strength, IS;[20] and electrolyte composition.[20,21] For some of these studies, it is difficult to find exact experimental conditions.

One observation, that is common to most of these studies, is that the velocity, as a function of the activity ratio, r, describes a bell-shaped curve, and the measured maximal velocity, V_{max}, for acute step growth is not the same as for obtuse steps. The calcite Ca:CO_3 ratio is 1:1, so for a given SI, one would expect the growth rate to be highest near $r = 1$. However, V_{max} has been reported near $r = 2$ for bulk calcite growth.[22] In contrast, V_{max} for the obtuse step is observed where $1 \leq r \leq 10$ and for the acute step, where $0.2 \leq r \leq 0.6$., for example, refs 16, 17, 20, 23, and 24. CO_3^{2-} attachment is considered to be the "growth limiting" ion for acute step growth because acute step advance is highest at high CO_3^{2-} activity. For the obtuse step, velocity is highest when Ca^{2+} is in excess, so Ca^{2+} activity is considered the "limiting ion" for obtuse step growth. We would like to stress that the saturation index is ultimately the controlling factor, but that the proportion of the ions plays an important role. Growth requires incorporation of both ions and their uptake depends on a number of simultaneous reactions. The processes of ion incorporation can be thought of as modifiers, i.e., the parameters that control step growth rate and not as "limiting" processes. Modifying processes include hydration, dehydration, attachment, and detachment. Thus, the influence of the local atomic structure at step edges determines which of the processes proceed rapidly and which are hindered. These effects combine to yield the overall rate. If one considers the average growth rate, the data from previous work indicates that obtuse step growth rate is increased by the sum of the processes in solutions, when Ca^{2+} ions dominate, and the rate of acute step growth is increased above the average when CO_3^{2-} ions dominate. Likewise the rate for each type of step decreases for cases where the rate of incorporation of one ion is hindered relative to the others.
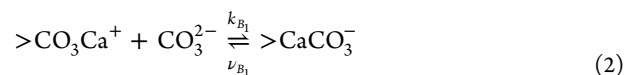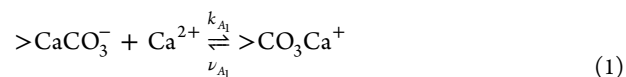
In none of the reports of previous work could we find clear evidence for *why* the obtuse and acute steps each grow fastest at different activity ratios. It has been explained by different dehydration frequencies for the Ca^{2+} and CO_3^{2-} ions and by the structural differences in attachment site spacing on the two types of steps,[25] which leads to (i) differences in attachment and detachment frequencies for the ions at the kink sites,[21,23] (ii) different attachment or detachment mechanisms for Ca^{2+} and CO_3^{2-},[24] and (iii) differences in the growth processes.[20,21] The goal of this work was to improve understanding about calcite growth processes and to explain the behavior observed both in our studies and the reports of others. We investigated the influence of (i) the Ca^{2+} to CO_3^{2-} activity ratio and (ii) the SI on calcite step growth. We measured calcite step velocities in systematic experiments over a range of SI (0.6, 0.8, and 1.0) and r (0.1−50). In contrast to some of the previous studies of this type, we ensured control on solution composition, to exclude velocity changes arising from changing ionic strength, electrolyte composition, or pH. Our extensive experimental data set includes many repetitions to account for variations in local crystal purity, defect density, and possible crystal distortion. We fitted our data with several existing process based growth models that vary in degree of complexity: Zhang and Nanchollas[26] (Z&N), Wolthers et al.[27] (WOL12), Wolthers et al.[25] (WOL13), and Stack and Grantham[24] (S&G). Our goal was to obtain sets of parameters that describe growth over a range of SI and that consider the structural

differences between the acute and obtuse steps. Lastly we correlated trends observed in the experiments and in the fitted model parameters to the atomic configuration and bonding arrangement on the calcite surface.

■ GROWTH MODELS

Several models have been proposed to predict calcite growth. However, most growth models have struggled to describe all of the trends observed in the experimental data, probably because of the complexity of competing processes that affect growth under the full range of possible physical−chemical conditions. Many of these could well be connected with the differences in atomic structure at acute and obtuse step edges. Ion attachment affinity based descriptions, which are derived from the measured growth rates relative to the saturation state in the solid−fluid system, break down where the solution composition differs from that used to calibrate the model and when growth is not a result of a single growth mode at a single type of dislocation.[13] Process-based growth models, which are built from conceptual models of the reactions thought to occur at the mineral surface, are often used to describe growth and dissolution of calcium carbonate compounds. For all of these reasons, we focused on exploring the match between data from experiments over a broad range of solution conditions and four process-based growth models, three of which are considered state of the art models.[28]

Step advance proceeds preferentially through the attachment of the constituent ions, in this case, Ca^{2+} and CO_3^{2-} or HCO_3^-, to high energy surface sites along step edges, in kinks or corner sites.[29] The attachment, k, and detachment, v, reactions of Ca^{2+} and CO_3^{2-} can be written as incorporation reactions:

$$>CaCO_3^- + Ca^{2+} \underset{\nu_{A_1}}{\overset{k_{A_1}}{\rightleftharpoons}} >CO_3Ca^+ \tag{1}$$

$$>CO_3Ca^+ + CO_3^{2-} \underset{\nu_{B_1}}{\overset{k_{B_1}}{\rightleftharpoons}} >CaCO_3^- \tag{2}$$

where > denotes a surface site, as in surface complexation modeling.[6,30−33] These reactions describe the reversible attachment of a growth unit (Ca^{2+} or CO_3^{2-}) and the transition from a Ca^{2+} surface site to a CO_3^{2-} surface site or vice versa, as the surface step grows or dissolves. To attach to a kink site, an ion has to diffuse through the solution and over the surface and then dehydrate.[34] Similarly, the growth site must dehydrate before it can accommodate an additional cation or an anion. In the pH range of our studies, HCO_3^{2-} is the dominant carbonate species, but according to Andersson et al.,[35] we can ignore HCO_3^{2-} attachment because protonation/deprotonation reactions are rapid and provided pH > 7, the carbonate ion has a lower free energy than the bicarbonate when it adsorbs on or forms part of a calcite surface. Also, we do not consider protonation of surface sites to be a limiting factor for growth because at these pH conditions, the majority of carbonate growth sites are deprotonated CO_3 species, for example, refs 19, 30, and 36.

In 1998, Zhang & Nancollas (called Z&N), presented the "kinetic ionic model", which describes growth and dissolution of ionic minerals, assuming cubic crystal structure, such as for NaCl. Their model includes the kinetic ion activity ratio (r_i):

$$r_i = \frac{k_A}{k_B} \frac{[A]}{[B]} \tag{3}$$

as a variable, in addition to the ion activity product. The kinetic ion model describes the availability of kink sites and is a function of the rate constants for incorporation, k, and the activities of the cation, [A], and anion, [B]. To maintain crystal stoichiometry, it is assumed that at equilibrium, the kink density for both sites is equal.

In spite of ignoring composition and structural differences for kink sites of noncubic crystals, as well as differences in the attachment, detachment, and dehydration frequencies between the anions and cations of soluble and sparingly soluble salts, this model continues as the foundation for current conceptual models.[28] Assuming equal dehydration frequencies for the various ions is particularly problematic because of the much slower water exchange rates for cations, especially divalent or multivalent ions, compared with anions.[29] This is why Christofferson and Christofferson[37] and later Wolthers et al.[27] assume that anion attachment is further limited by dehydration of surface cations.

Wolthers et al.[27] modified the Z&N kinetic ion ratio model, by adding a surface complexation component,[33] and they extended the binary model to a ternary model, by incorporating HCO_3^- ions. Their process based growth model (called WOL12) incorporates aspects of solution composition as well as attachment and detachment frequencies for various configurations of surface sites, to calculate flux balance. These are used to determine kink formation and propagation rates, which give the crystal growth rate normal to the surface. The modified kinetic ionic ratio in the WOL12 model is

$$r_i = \frac{\overline{k}_A \overline{\nu}_B \; [A]}{\overline{k}_B \overline{\nu}_A \; [B_1]} \tag{4}$$

where $\overline{k}_i$ and $\overline{\nu}_i$ represent the effective attachment and detachment frequencies for the cation, A, in this case Ca^{2+}, and the anion, B, which is $CO_3^{2-\bullet}$, and they also account for pH dependence. The model differentiates between CO_3^{2-}, B_1, and HCO_3^-, B_2, sites and includes variable proportions of face, edge, and corner sites. A value for the fraction of potential growth sites, χ, is calculated from surface complexation modeling and is the sum of kink density for the various possible surface sites at the mineral-solution interface. The model is, however, still based on a cubic crystal lattice; i.e. it does not consider calcite step geometry. For the calculation of kink density, the model uses identical formation energies, ε, i.e., $\varepsilon_{obtuse} = \varepsilon_{acute} = \varepsilon$, for the various kink site types.

Later, Wolthers and colleagues[25] refined and updated the fit parameters of their model. They found that water exchange frequency depends on the calcite step type, so they included the frequency of kink formation and Ca^{2+} attachment and noted that the attachment of HCO_3^- and CO_3^{2-} is controlled by surface Ca^{2+} dehydration. This modified model (called WOL13) still includes identical kink formation energies for both the acute and the obtuse step ($\varepsilon_{obtuse} = \varepsilon_{acute}$), but it does account for different atomic configuration of the steps through different attachment frequencies.

An earlier growth model was developed specifically for calcite by Stack and Grantham[24] (called S&G). It includes fewer parameters and is much less complex. It assumes that calcite surface growth solely depends on the rate of kink site nucleation and the rate of attachment for Ca^{2+} and CO_3^{2-} ions. The attachment rates are treated independently and depend on the ion concentrations. One constant is used to describe the overall detachment rates, and recently this has

been shown to approach zero[17] and hence is small enough to be neglected in the model.

■ METHODS

Although temperature and pressure play a role in the rate of calcite growth, we chose to work at standard conditions, i.e., $T = 25\ °C$ and $P = 1$ atm, so we could compare our results with previous studies; experiments at room temperature have fewer sources of experimental uncertainty, and it would narrow the number of variables and would provide data for all of the environments at ambient temperature where calcite grows, both naturally and for commercial purposes. A detailed description of the experimental set up and spiral growth step advance measurement is presented in Larsen et al.[23] and is summarized below.

Materials and Solutions. Spirals were grown on freshly cleaved Iceland spar calcite crystals using the same flow through set up as described by Larsen and colleagues.[23] Single crystals were cleaved immediately before each experiment to minimize recrystallization and contamination by adventitious hydrocarbon, resulting from air exposure.[8,38] Cleaved crystals ($4 \times 4 \times 3$ mm) were swept with a jet of pure N_2 gas, to remove loose calcite particles from the cleaved surfaces. Care was taken to avoid contamination by silicate (from glass vessels) and hydrocarbons (from air and solution). The standard experiment solutions were designed to keep constant pH (8.5 ± 0.1), ionic strength (0.1 M KCl), and temperature ($25 \pm 1\ °C$) to test the effect of different Ca^{2+} to CO_3^{2-} activity ratios ($r = 0.1, 1, 10, 25,$ and 50) and varying saturation indices (SI = 0.6, 0.8, and 1.0), where

$$SI = \log\left(\frac{\text{ion activity product}}{\text{solubility product}}\right) = \log\left(\frac{IAP}{K_{sp}}\right) \tag{5}$$

The solution speciation for each experiment was determined using PhreeqC,[39] with the phreeqc.dat database and the calcite equilibrium constant, $K = 10^{-8.48}$, from Plummer and Busenberg.[40] The experimental Ca^{2+} and CO_3^{2-} solutions (described as MIX1 and MIX2 in Figure 3 of ref [23]) were prepared using stock solutions made from reagent grade chemicals and ultrapure water, deionized with a Milli-Q ion exchange column. Solutions contained 1 M $CaCl_2$, 1 M $KHCO_3$, 3 M KCl, 0.1 M KOH. The 1 M $KHCO_3$ solution was freshly prepared just before the spiral growth experiment to minimize decrease in dissolved carbon as a result of degassing, particularly at high CO_3^{2-} concentrations, i.e., $r < 1$.[23] All other stock solutions were prepared and used for multiple experiments. Solutions stored in polypropylene bottles that had been rinsed with hot water to minimize hydrocarbon contamination.[38]

Growth Experiments. The Ca^{2+} and CO_3^{2-} solutions were prepared from the stock solutions that were made using information from predicted solution speciation (Supporting Information, Table 1) and transferred to the MIX1 and MIX2 reservoirs (300 mL Teflon screw cap jars) and sealed. The solutions were pumped, using a multichannel peristaltic pump calibrated to a flow rate of 0.6 mL/min per channel, from the reservoirs to the small (25 mL) Teflon reaction cell that contained two or three freshly cleaved calcite crystals. This resulted in a total solution flow of 1.2 mL/min in and out of the reaction cell, where the solution was continuously mixed by a magnetic stirrer. Each experiment began with an initial set of solutions with SI = 1.0 and $r = 1$ or 10, to ensure rapid spiral

growth. After ~45 min, the solutions in MIX1 and MIX2 were exchanged with solutions made to fit the selected experimental conditions (Supporting Information, Table 1), and pumping continued for another 25−140 min, depending on step growth rate. At the end of the experiment, the calcite crystals were removed from the reaction cell. The remaining water was mechanically removed with a jet of N_2, and the resulting droplet at the edge of the crystal was wicked away with the corner of a dust free tissue (kimwipe) to minimize the evaporation of residual solution.[38] The time between solution exchange and crystal removal was recorded. Before, during, and after the experiments, small aliquots were taken from MIX1, MIX2, and the reaction cell to verify pH, Ca, and CO_3 concentrations. Ca concentration was measured using a PerkinElmer AAnalyst 800 atomic absorption spectrometer (AAS), pH was measured using a Metrohm NTC pH glass combination electrode calibrated with NBS standard buffers, and CO_3^{2-} concentration was determined using a Metrohm 785 DMP Titrino titrimeter.

Analysis of Spiral Growth Pyramids. The dried crystals were placed on a glass slide for differential interference contrast (DIC) microscopy to determine absolute growth velocities for the obtuse and acute steps, by the method described in Larsen et al.[23] In short, if the step spreading velocity on the acute and obtuse sides is identical, symmetrical pyramids form, with apex angle, $\theta = 180°$. This is generally observed when the Ca^{2+}:CO_3^{2-} activity ratio, r, is close to 1. When the velocities of acute and obtuse steps are different, asymmetrical pyramids form, with apex angles greater or less than 180°. This occurs when $r \neq 1$. When the solution producing the initial pyramid is changed, the pyramid shape changes immediately, thus marking the start of pyramid growth under the new set of conditions (gray vs black outlined pyramid in Figure 1a). Using DIC, we measured the distance (x) from the pyramid apex to the intersection of the obtuse and acute steps at the corners of the pyramid and the angle θ between the obtuse−acute and acute−obtuse ridges on the pyramid (Figure 1b,c). From these measurements, the growth velocities for the obtuse (v_o) and acute (v_a) steps were determined with the relationships:

Figure 1. (a) Diagram modified from Larsen et al.[23] showing the change in pyramid geometry from gray to black after the solution composition was changed from that used to initiate spiral growth. The diagonal gray line marks the obtuse−acute ridges on the pyramid and because the line is straight, the angle, θ, between the ridges is 180°. The black rhomb show the resulting pyramid for a growth solution where $r = 1$, i.e., $\theta \neq 180°$. The length of a ridge and the angle between the ridges are used to determine the velocities for each type of step following eqs 6 and 7. (b, c) typical DIC microscope images showing the measured length (red line) and angle (θ); they are 60 μm square.

$$v_o = \sin\left(\frac{\theta + \gamma}{2}\right) x t^{-1} \tag{6}$$

$$v_a = \sin\left(\frac{\theta + \gamma}{2}\right) x t^{-1} \tag{7}$$

where γ represents the angle between two equivalent step edges (101.6° for the {10.4} calcite face), and t represents the time between the point where the system is at equilibrium after solution exchange to the end of pyramid growth, when the experiment ended.

Each set of experimental conditions was tested at least three times, where each replicate experiment was conducted on a different day, using freshly cleaved crystals and fresh solutions. We measured 10−30 pyramids for each experiment, resulting in 30−100 measurements for obtuse and acute step velocity per tested condition. This provided enough data to statistically minimize the effects of slight differences in conditions or in the types and density of crystal defects in the cleaved Iceland spar substrates. We note that with DIC we could not distinguish pyramids that originated from a single source spiral from those with a more complex dislocation source. According to Teng et al.,[13] steps on spirals that form at single dislocations grow more slowly than steps from a more complex origin. This likely accounts for the spread in our data.

■ FITTING

We added a smoothing spline fit to the experimental data to visualize some general trends (Figure 2). The smoothing spline fit reduces the influence of uncertainty in the data and avoids overfitting. We chose this mathematical model because it has no underlying assumptions about the curve shape.

To obtain kinetic parameters for step growth as a function of SI and r, we fitted four growth models to our data: Z&N (Zhang and Nancollas[26]); WOL12 and WOL13 (Wolthers et al.[25,27]) and S&G (Stack and Grantham[24]). We used the equations from the articles, but we fitted the data individually for the acute and obtuse steps, to give specific values for each so as to account for possible differences in growth velocity resulting from geometric and structural differences for the two step types. Ideally, for the WOL12/13 models, values for growth sites (χ) for each individual experimental condition that were obtained through surface complexation modeling are required. This is beyond the scope of most studies so we tested the Wolthers models using (a) the reported mean χ value ($\chi = 0.01$) estimated in Wolthers et al.[27] from the experimental conditions[21,13,24] and (b) the calculated χ values using the CD-MUSIC model from our experimental solution. For the latter approach, we used the surface model developed for divalent metal carbonates[33] which is based on the CD-MUSIC model.[41,42] For those results to be applicable to this study, we calculated the empirical relationship between χ and r, which allowed us to present the velocity data as a function of r.

Previous studies have shown that at SI ≤ 0.8, 2D growth is negligible,[13] but at SI = 1, 2D growth needs to be considered.[43] To account for possible changes in growth mechanisms, we used two approaches for fitting our experimental data: (1) a Fit All approach where all the step growth data obtained at the three different SI (SI = 0.6, 0.8 and 1.0) was fitted using *one* set of parameters for each step and (2) a fit 0.6−0.8 approach where the step growth data obtained at SI = 0.6 and 0.8 were fitted and the derived parameters were used to constrain the growth velocity curve for the data obtained at SI = 1. We
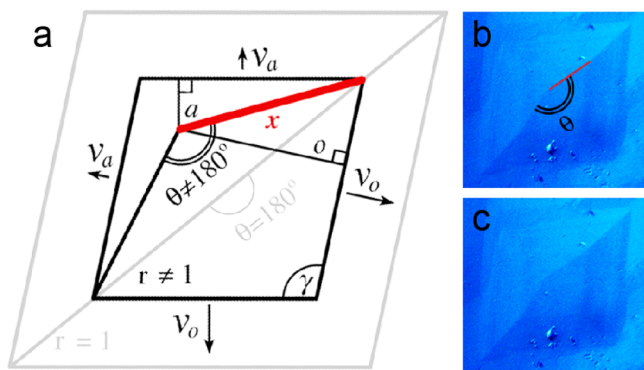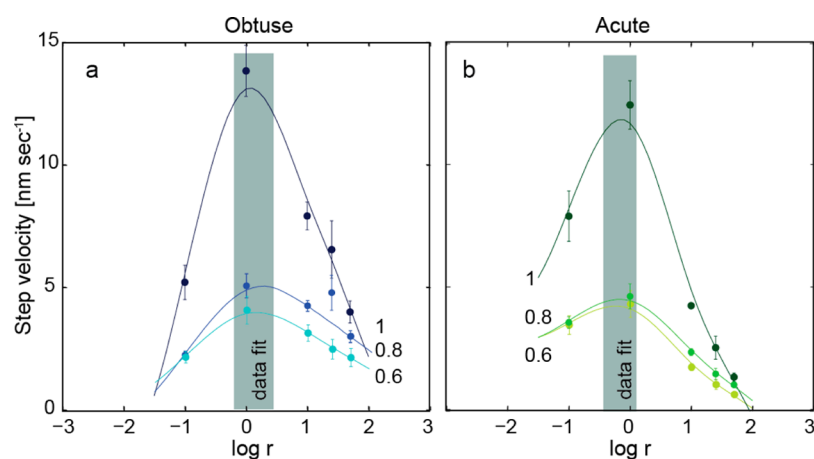
Figure 2. Experimental step velocity data (points) for the (a) obtuse and (b) acute step at a range of r, $Ca^{2+}:CO_3^{2-}$ activity ratio and SI, (determined using eqs 5 and 6) and fitted with a smoothing spline (lines). The dark gray bars show the r range over which V_{max} varies as a function of SI.

Table 1. Average Measured Growth Velocities in nm/s for Obtuse and Acute Steps at Various $Ca^{2+}:CO_3^{2-}$ Activity Ratios (r) for n, the Number of Spirals Examined

	SI	0.60			0.80			1.00		
r	velocity	nm/s	lstd	n	nm/s	lstd	n	nm/s	lstd	n
0.10	obtuse	2.2	0.2	122	2.2	0.2	35	5.2	0.7	83
	acute	3.5	0.4	122	3.6	0.2	35	8.0	1.0	83
1.00	obtuse	4.1	0.5	51	5.1	0.5	18	13.8	1.0	101
	acute	4.3	0.5	51	4.6	0.5	18	12.5	1.0	101
10.00	obtuse	3.2	0.3	31	4.2	0.2	34	7.9	0.5	43
	acute	1.7	0.1	31	2.3	0.1	34	4.3	0.3	43
25.00	obtuse	2.5	0.4	35	4.8	0.7	21	6.5	0.8	51
	acute	1.0	0.2	35	1.5	0.2	21	2.6	0.3	51
50.00	obtuse	2.2	0.4	46	3.0	0.2	41	4.0	0.4	41
	acute	0.6	0.1	46	1.0	0.1	41	1.4	0.2	41

implemented the fitting procedures using Matlab R2012b, where model step velocities were determined for each individual set of experimental conditions. The residual sum of squares (RSS) between modeled and measured rates was minimized by adjusting the model parameters. The minimization process used the trusted-region-reflective algorithm[44] and the tolerances for the change in parameters and function value were set to 10^{-15}. Gradients were estimated using central finite differences. Because of the nonlinear nature of the underlying models, we cannot guarantee that the presented parameters constitute a global optimal set of parameters. However, a further investigation using stochastic fitting methods of the type proposed by Storn and Price[45] did not improve the fit. This provides confidence about the output of the fitting procedures.

■ RESULTS AND DISCUSSION

In all the experiments, steps grew predominantly from dislocation defects, which produced single- or multiple-sourced growth spirals. Consistent with previous reports,[16−20,23,24] growth velocities for the spirals are significantly influenced by the $Ca^{2+}:CO_3^{2-}$ activity ratio (r) in solution and the saturation index (SI). The average step velocity for each step is shown in Table 1 for each SI, r and number of spirals measured (n). The measured growth velocities for the acute and the obtuse step as a function of r and SI, along with a modeled smoothing spline, are shown in Figure 2. The data point for the obtuse step at SI = 0.8 at r = 50 is an experimental outlier and is excluded from the spline and model fits. Our results show some general

trends: (i) growth rate increases with increasing SI, (ii) the peak width decreases with increasing SI, (iii) V_{max} is not the same for obtuse and acute steps, (iv) there is an asymmetric decrease in step growth when Ca^{2+} dominates in solution and this is different when CO_3^{2-} dominates and (v) there is no detectable change in the $Ca^{2+}:CO_3^{2-}$ activity ratio, r, associated with V_{max}, as SI changes, for either type of step (Figure 2).

We discuss these features in turn.

(i) Increase in growth rate with increasing saturation index. Figure 2 shows slightly higher velocity for SI = 0.8 than for 0.6 and a considerable increase in step velocity at SI = 1. An increase in rate is expected with increasing SI because of the increased driving force for precipitation. The logarithmic dependence of SI (SI = log(IAP/Ksp)) makes the step between each saturation state look similar, however the IAP is increased by 1.5 from SI = 0.8 to 1 compared to only 1 from SI = 0.6 to 0.8. Therefore, a higher velocity increase is expected when SI is increased from 0.8 to 1.0 than from 0.6 to 0.8.

(ii) Peak width decreases as SI increases. Hellevang and colleagues[28] correlated the width of the step velocity curves (as a function of r) with the number of possible incorporation sites for the individual growth units. In this case, the narrow peak width at high SI means that there are few possibilities for incorporation, and the wider curves for SI = 0.6 and 0.8 show that there are many possibilities for growth unit incorporation. This means that growth is not hindered at high SI and kinks are constantly being created. At lower SI, ions are in shorter supply for the many available kinks so growth is slower.

(iii) V_{max} is not the same for obtuse and acute steps. The maximum velocity for the obtuse steps occurs at a different ion activity ratio than for acute steps (gray bars in Figure 2). The acute step velocity peaks when dissolved CO_3^{2-} is slightly in excess (Figure 2) for all three SI conditions and the obtuse step velocity is highest when Ca^{2+} is slightly in excess. Although obtuse steps grow faster when $r > 1$, conditions when dissolved carbonate dominates result in acute step growth outcompeting obtuse step growth.

(iv) Asymmetric decrease in step growth when Ca^{2+} dominates in solution compared to when CO_3^{2-} dominates. In spite of the few data points at low r, it is clear that acute step growth decreases more slowly at lower SI conditions, whereas the reverse trend is observed for obtuse step growth (Figure 2a,b). This shows that acute growth rate is more sensitive to r at low CO_3^{2-} activities and obtuse growth rate is sensitive to r at low Ca^{2+} activities. Although the agreement between velocity measured at $r = 1$ and the smoothing spline fits are not perfect at SI = 1, it is more symmetric. This is probably explained by the higher activity of ions and hence, the modifying effect of incorporation of one ion rather than the other ion plays a lesser role.

(v) There is no detectable change in the $Ca^{2+}{:}CO_3^{2-}$ associated with V_{max} as SI changes for either type of step. Within the resolution of our data, the smoothing spline fits do not indicate a change in r for the acute and obtuse V_{max} as SI varies (Figure 2). However, the smoothing spline fits for the SI = 0.6 data indicate that the acute step has a slightly higher V_{max} than the obtuse. For SI = 0.8 and 1, the obtuse V_{max} is higher than the acute V_{max}, which matches most previous experimental studies on calcite step growth.[16−20,23,24]

Larsen and colleagues[23] examined step growth rate as a function of r and also reported higher maximum velocity for the acute step at SI = 0.6. Their values for $r = 0.1$ were higher than ours but they remarked that results obtained at $r < 1$ are somewhat uncertain because of the possible loss of CO_3^{2-} at high CO_3^{2-} activity in contact with air (Supporting Information).

■ MODEL TESTING

The smoothing spline fits show trends but give no information about growth kinetics and mechanisms. Therefore, we fit our data with four growth models in an attempt to obtain information about attachment and detachment frequencies. We used 4 proposed growth models Z&N,[26] WOL12,[27] WOL13,[25] and S&G.[24] We could not obtain a good fit using the parameters reported. This is not surprising because our experimental data were obtained at different chemical conditions than the data used to derive the model parameters, such as the range of SI (0.06−0.62[13] and 0.34−0.43[24]) and pH (7−9[24]). Also, the original Z&N and the WOL12 models did not provide separate parameters for the obtuse and acute steps, whereas in our study, we used the models to fit the step types separately. The resulting velocity curves from the WOL12 and WOL13 models were overlapping, giving only slight differences in parameter values. Therefore, we do not distinguish between them further in the following discussion on the relationship between velocity and r. In the first part of the Results section the WOL12/13 data were obtained used the average χ value of 0.01 for all the experimental solutions.[27] Results of a text on the influence of this assumption are presented below.

It was expected that the Fit All approach could be problematic because when SI = 1, 2D growth is no longer

negligible.[43] Indeed, fitting all SI data at once (but separately for the acute and obtuse steps) did not produce a good fit with any of the models. The predicted velocities from the Fit All approach are shown in Figure 3. All models fail to account for
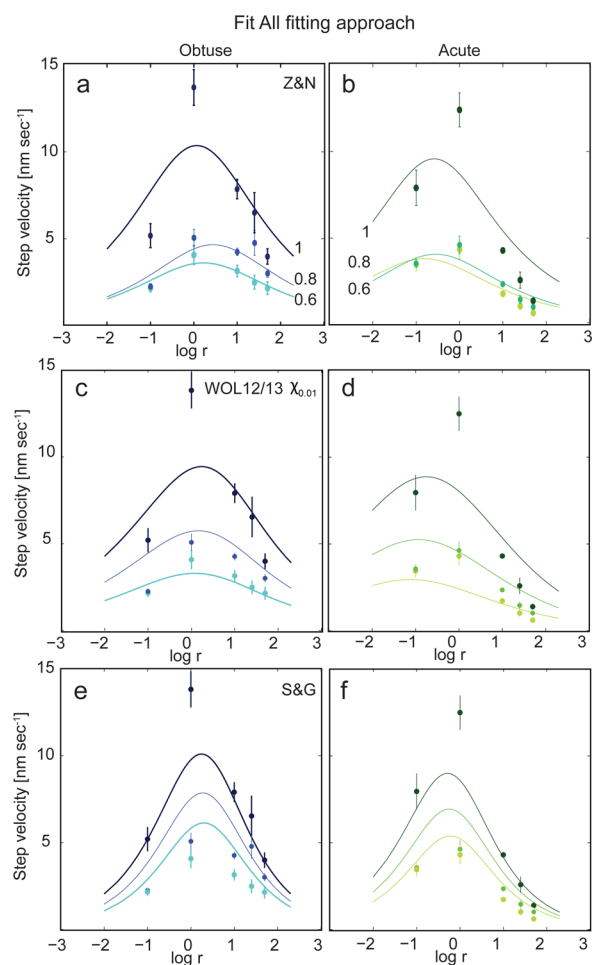

Figure 3. Our data fit with the models for obtuse (blue) and acute (green) step growth, at the three saturation indices, using the Fit All approach where the experimental data are fitted to one set of parameters. (a) The Z&N model for the obtuse step edge growth rates, (b) Z&N, for the acute step edge growth rates, (c) WOL12/13, obtuse, (d) WOL12/13, acute, (e) S&G, obtuse, (f) S&G, acute. The SI relationship to the color code is indicated in parts (a) and (b).

the high velocity points where r is close to unity. Only the S&G model predicts a curve shape somewhat overlapping the trend of the experimental data but the model overestimates the velocities for SI = 0.6 and 0.8. A much better fit to all models is obtained when the SI = 1 data are excluded from the fit and the parameters obtained with the fit 0.6−0.8 are used to calculate the model curves for the SI = 1 data (Figure 4). The detachment and attachment frequencies obtained from the model fits to the SI = 0.6 and 0.8 data are presented in Table 2, along with the estimated errors. A full table of fitted and calculated parameters for all procedures is given in Supporting Information, Tables 2 and 3.

In general the fit 0.6−0.8 approach using the Z&N and WOL12/13 models leads to a good match with the experimental data at higher r values (Figure 4a,b and c,d) and a reasonable match for the obtuse step. Larsen and colleagues[23] also found the Z&N model to reasonably describe
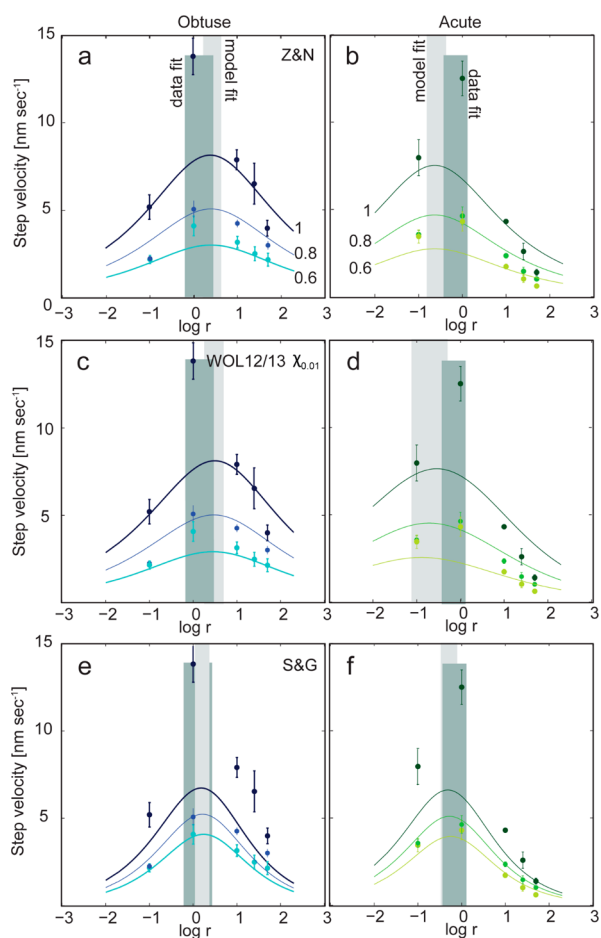
Figure 4. Model fits for the obtuse (blue) and acute (green) step growth data using the Fit 0.6–0.8 fitting approach, where the parameters derived from fitting the data obtained at SI = 0.6 and 0.8 were used to generate the model curves for SI = 1. (a) Z&N model fit to the obtuse step growth rates and (b) Z&N for the acute step data, (c) WOL12-13, obtuse, (d) WOL12/13, acute; (e) S&G, obtuse, (f) S&G, acute. The dark and light shaded bars indicate the domain for V_{max} for all SI, from the data and the smoothing spline fit. Error bars represent one standard deviation on the experimental data (circles). The SI relationship to the color code is indicated in parts (a) and (b).

their obtuse step data. None of the models fit the high velocity data (log r = 0) for the acute steps or for either types of steps at SI = 1, where measured velocities are considerably higher than those predicted by refitted Z&N or WOL12. For both types of step, the models fail to predict V_{max}, resulting in a peak that is skewed relative to the experimental data. The range of ion activity ratio, where step velocity is at a maximum for the tested models, and the spline fits are illustrated in Figure 4, where the dark gray bar represents the predicted location for V_{max} for all SI from the smoothing spline fits and the light gray bar shows the range for V_{max} predicted by the models. For the obtuse step, the model fits predict V_{max} at slightly higher r than the smoothing spline fits, while for the acute step, modeled V_{max} is at considerably lower r than for the smoothing spline fits (Figure 4b,d). The S&G model gives a better fit for SI = 0.6 and 0.8, at near stoichiometric conditions, than the Z&G and WOL12, where it manages to include the measured high velocity points at log r = 0. S&G predicts a narrow range for the position of V_{max}, which overlaps with the smoothing spline fit prediction. However, in contrast with the other two models,

S&G cannot simulate the SI = 1 experimental data (Figure 4e,f) and underestimates velocities. S&G is better at constraining the high velocity data for the acute step but it also fails to describe the data for SI = 1. The Z&N and WOL12/13 models cannot reproduce the experimental data, probably because of the assumptions that are required. The Z&N model was made for cubic, two ion crystals and uses attachment frequency as a function of activity to model growth rate. It is unable to account for the nonequivalent occurrence of the maximum step velocity for the two step geometries. The WOL12 formulations do not account for step geometry differences either, and are fitted to data with varying SI and pH which are known to change the step velocities.[16−18,20,24]

We made a sensitivity analysis to test if the performance or the Wolthers models would depend on the applied growth site fractions. First we changed the χ values ± a factor of 1 from the value of χ = 0.01 as estimated for a narrow range of experimental conditions in Wolthers et al., 2012. In this case the fitted parameter values change with χ, but the resulting curve fits were basically identical to the one with χ = 0.01. Then we compared the calculated vs the measured velocities with both χ = 0.01 and the correct χ values obtained with CD-MUSIC modeling for each of the experimental solutions (Supporting Information, Figure 1). This comparison shows that the previously used value of 0.01 overestimates the calculated growth for our experimental conditions, stressing the need to combine CD-MUSIC modeling with application of WOL12/13. However, obtaining the calculated χ values with the CD-MUSIC model for our solutions did not improve the subsequent refit to the model curves. The calculated χ values increase as a function of SI for our experiments except for SI = 0.6, where the χ value at r = 0.1 is higher than for SI = 0.8 and 1 (Supporting Information, Figure 2). Using an empirical relationship between χ and r, we accounted for the changing χ values across our solution compositions in the fitting procedure. The empirical relationship between χ and r is off for SI = 0.6 relative to the other solution compositions and returned a poor fit for SI = 0.6 (Figure 5a–d). Hence we used the Fit All approach to assess the importance of applying the correct χ values to the Wolthers models. In contrast to our expectations, the resulting curve fits were similar and only the parameter values changed as observed in the sensitivity analysis (Figure 5a,b) for the curve fits. The curve fits obtained with the WOL12/13 are compared in Figure 5c,d.

The similarities of the fitted curves for all models and the behavior of the optimal parameters with respect to changing χ values for the Wolthers models indicate that the equations contain some inherent nonuniqueness for the energy and rate parameters in all of the tested models, as previously discussed.[27] Also, the curve heights for all the fits are strongly influenced by the detachment rates. In theory, the detachment rate should not have a big influence on the rates because the experiments were performed at supersaturated conditions. Moreover, by visually inspecting the dependence of the velocity curves on the parameters, their shape and location is restricted in all models. The shape restriction possibly prevent the models from describing the high velocity data (Figure 4).

One of the objectives of this study was to use the fitted and calculated parameter values for the frequencies of attachment and detachment to evaluate the differences between the obtuse and acute steps. However, the poor performance of the models to fit our experimental data does not allow us to consider the parameters from the fitting procedures as absolute values. Still,

Table 2. (a) Fitted Parameter Values Derived from the Four Models Using Our Experimental Results for SI = 0.6 and 0.8, at All Activity Ratios and the Parameter Abbreviations That Were Used in the Original Papers and (b) Schematics Showing Which Steps Have the Highest Values for the Most Relevant Fitted and Calculated (Italic) Parameter Values[a]

(a)				
Z&N	ε^*	kA	kB*	
obtuse	2.59×10^{-20}	1.98×10^{7}	4.91×10^{7}	
acute	2.43×10^{-20}	4.07×10^{7}	9.49×10^{6}	
Wol12	ε	kA		vA*
obtuse	1.49×10^{-20}	8.59×10^{7}		1.05×10^{4}
acute	1.53×10^{-20}	8.96×10^{7}		6.42×10^{4}
Wol13	ε^*			vA*
obtuse	2.39×10^{-20}			9.28×10^{4}
acute	2.62×10^{-20}			9.05×10^{5}
Wol12_χ	ε	kA		vA*
obtuse	1.84×10^{-20}	8.60×10^{7}		2.50×10^{3}
acute	1.91×10^{-20}	8.64×10^{7}		1.31×10^{4}
Wol13_χ	ε^*			vA*
obtuse	2.74×10^{-20}			2.22×10^{4}
acute	3.01×10^{-20}			1.92×10^{5}
S&G		k_Ca*	k_CO$_3$*	
obtuse		1.75×10^{6}	1.10×10^{5}	
acute		2.80×10^{6}	6.11×10^{4}	

(b)	ε	kA	kB	vA	vA$_2$	vB$_1$	vB$_2$
Z&N	acute	n.a.	obtuse	n.a.	n.a.	n.a.	n.a.
Wol12	n.a.	n.a.	n.d.	acute	acute	obtuse	obtuse
Wol13	obtuse	n.d.	n.d.	acute	acute	obtuse	obtuse
Wol12_χ	n.a.	n.a.	n.d.	acute	acute	obtuse	obtuse
Wol13_χ	acute	n.d.	n.d.	acute	acute	obtuse	obtuse
S&G	n.a.	acute	obtuse	n.a.	n.a.	n.a.	n.a.

[a]A full table with fitted and calculated parameter values is presented in the Supporting Information. ε represents kink formation energy [J]; k and v is the attachment and detachment frequency of the A and B ions: Ca^{2+} and CO_3^2 [s^{-1}]. A_2 indicates Ca detachment from a HCO_3^- site and B_1 and B_2 indicate detachment of CO_3^{2-} and HCO_3^-. * and mean that the calculated parameters differ between the obtuse and acute steps with 2 standard deviations. n.d.: no difference; n.a.: not applicable because no value was obtained for the given model.

they do provide relative rate information for comparing which processes have the strongest effect on acute and obtuse step growth. The fact that not all of the fitted parameter values are statistically significant highlights the caution that is required when applying models to experimental data in this system. Table 2b summarizes which step has the highest value for the kink formation energy and the attachment and detachment rates. According to the Z&N and S&G models the obtuse step incorporates CO_3^{2-} at a faster rate than the acute step. The WOL12/13 models support a faster detachment of Ca on the acute step and a faster detachment of CO_3 at the obtuse steps. However, we do not place much emphasis on the detachment frequencies because they are orders of magnitude smaller than the attachment rates and therefore do not play a significant role in the processes at the calcite surface.

To help resolve the discrepancy between observed and calculated rates for the acute and obtuse steps, we examined the orientation of the atoms at the step edges. Figure 6 shows the atomic structure of calcite where the position of CO_3 and Ca can be seen. The CO_3 groups and the octahedral O coordination around Ca alternate in orientation along step edges so each alternating site has its own distinct geometry (also refs 8, 38, and 46). Carbonate is marked as Ac_1 & Ac_2 on the acute corner and Ob_1 & Ob_2 at the obtuse corner. At the Ac_2, Ob_1 and Ob_2 carbonate sites, all oxygen atoms are fixed in the calcite structure with two O bound to one Ca and a third O bound to two Ca atoms. The Ac_1 group, however, i.e., every

second CO_3^{2-} on acute steps, has one O atom from the calcite structure free. Hence, the ion that attaches at the Ac_1 group can more easily adapt its orientation than for the Ac_2, Ob_1, and Ob_2 sites. This would influence attachment rates for the Ac_1 groups. It is likely that the ions can attach more easily at the Ac_1 site but they are also more exposed to attack by Brownian motion of the water molecules and pairing with other ions. Likewise, Ca^{2+} can attach and also detach more easily from the acute steps (cf. ref 41).

The insight gained from the three-dimensional atomic structure, together with a few trends in the model derived parameters, allows us to address the implications of the atomic arrangements a little further. The information from the fitting parameters that we are most confident of is the observations from the Z&N and S&G models that obtuse steps incorporate CO_3^{2-} at a faster rate than acute steps. In addition, the S&G model shows that the acute step incorporates Ca^{2+} fastest (Table 2). These rate observations combined with the atomic structure analysis leads us to interpret that (1) the less rigid CO_3 configuration at the acute step (Ac_1) decreases CO_3^{2-} attachment rate compared with the obtuse step; and (2) that either the more exposed configuration of attaching Ca^{2+} at the acute sites or the Ac_1 configuration enhances its attachment rate relative to Ca^{2+} at the more protected obtuse step. Dehydration is also likely to play a role in the kinetics of step growth. Molecular Dynamics (MD) simulations[25,47] report a lower water density near the acute step and higher dehydration
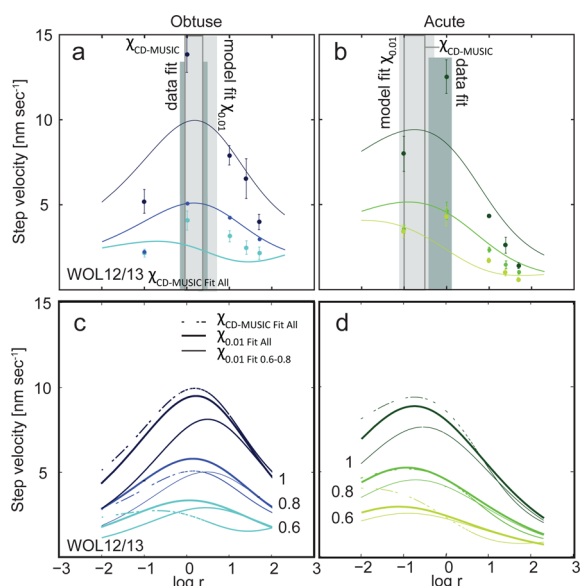
Figure 5. Experimental data (dots) fitted with the WOL12/13 model (lines) using the χ values calculated from the CD-MUSIC model for the obtuse (a, c) and acute (b, d) steps. (a, b) Resulting curve fits using the Fit All approach. The dark and light shaded bars in a and b indicate the domain for V_{max} for all SI, from the smoothing spline fit. The modeled data with the bar for $\chi_{CD\text{-}MUSIC}$ is outlined with darker gray. (c, d) are direct comparisons of the modeled curve between $\chi_{CD\text{-}MUSIC}$ (dashed) and $\chi = 0.01$ for the obtuse and acute steps. Error bars represent one standard deviation on the experimental data (circles) and SI is indicated.
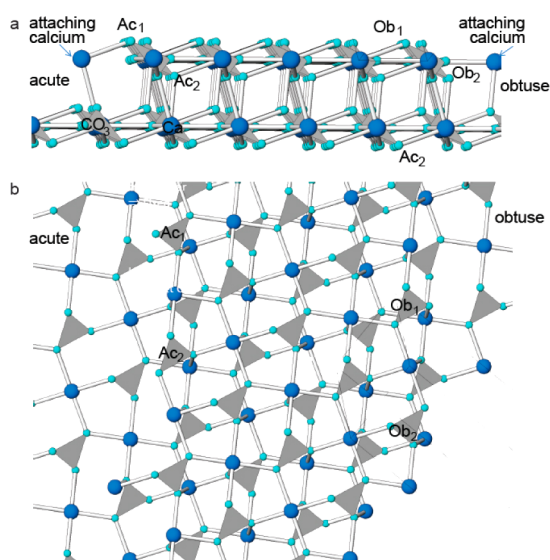
Figure 6. (a) View of an acute step, Ac (left) and an obtuse step, Ob (right). There are two alternating orientations for the CO_3 groups on the calcite edges: 1 and 2, just as there are two configurations for the oxygen coordination around calcium. This results in alternating coordination environments for adsorbing species. (b) Top view of the calcite steps showing the two orientations of CO_3 (1 and 2) at the acute (Ac) and obtuse (Ob) steps. The oxygen coordination around the Ca atom likewise alternates. Gray represents CO_3; bright blue, oxygen; dark blue, Ca^{2+} (generated by the software Atoms).

frequency of calcium ions within acute steps. Since Ca^{2+} is most rapidly incorporated at the acute step (b) we can now also conclude that (3) dehydration of Ca^{2+} can cause a slower Ca^{2+} supply relative to CO_3^{2-} at the obtuse step. This would cause

the obtuse step to grow faster in Ca^{2+} rich solutions (as we see in Figures 2, 3, and 4). If the water exchange rate for surface calcium ions limits carbonate ion attachment, these simulation results would imply that CO_3^{2-} attachment to Ca in an obtuse step is slower than to Ca in an acute step. We see the opposite from our model fits. Most likely, the difference in geometry of the steps affects CO_3^{2-} attachment more strongly than, or as well as, cation dehydration at the steps. It is likely that dehydration frequency of Ca^{2+} affects the rate of progression of both steps but because of the slower attachment of CO_3^{2-} at the acute step, the dehydration rate of Ca^{2+} plays a larger role at the obtuse step, where CO_3^{2-} ions are incorporated at a higher rate (Table 2, kB from Z&N and k_CO_3 from S&G).

Ca^{2+} dehydration modifying the obtuse step rate is consistent with previous results.[20,21,23] The processes reported to be important for enhancing acute step growth rate include controls by dehydration rate at carbonate sites for calcium attachment,[19] and adsorption and surface diffusion rather than diffusion in solution.[20] Considering the local oscillating charge on calcite surfaces with both negatively and positively charged surface sites, we expect a high barrier to diffusion on the surface and infer that diffusion in solution would dominate over diffusion at the surface (cf. ref 20). We consider it most likely, however, that it is the atomic arrangement of the calcite steps, together with calcium dehydration rate that determines the differences in velocity and ion preference for the two types of steps and that dehydration of ions and the surface has an important influence on the measured velocities. An interplay of processes, which would each be influenced by the particular experimental conditions to different degrees, would each contribute, resulting in the differences we observe in the published experimental data sets.

Our results clearly demonstrate the need for a conceptual model to describe what happens when ions attach on a surface and a chemical—physical model that can describe calcite step velocity that fits for the various experimental conditions. Our way forward was to consider parameters for the incorporation processes for each of the acute and obtuse steps individually. From our experimental data, it is clear that a more rigorous model would incorporate the influence of Ca^{2+} dehydration for the velocity of obtuse steps and the less rigid orientation of the trigonal planar CO_3^{2-} ions at the acute step, for describing the decreased anion incorporation rate. Also the sensitivity of the velocity, especially to dissolved ion activity ratio and pH[20,27,48] illustrates that solution speciation should be accounted for in the models. The failure of the models to describe our data could also indicate that there is a yet undescribed growth mechanisms at play that is not accounted for in the numerics of the models, e.g., the switch to 2D nucleation at conditions where stoichiometry is at or close to 1:1 Ca to CO_3, even at SI = 0.7, has previously been observed (personal communication, Gernot Nehrke). Also current growth models only consider addition of individual ions despite that several papers present evidence for the presence by higher order $CaCO_3$ species, for example, refs 49 and 50.

Our study also demonstrates that the assumption of kink density for both types of sites being equal is not always valid. The SI dependent variation of the width of the velocity peaks, as a function of r, combined with the distinctly different r values for the V_{max} for the two types of steps indicates that the number of active sites is quite likely not a ratio of 1:1 but rather, it also varies with step type and solution conditions. Other interesting parameters to take into consideration are the structure in the

solution around a nonflat surface and the terrace width, i.e. the distance to the closest steps or defects. Sand et al.[51] found a far reaching influence of step structure, out into the fluid in the calcite−alcohol−water system. Water was repelled from terraces where ethanol was ordered but at steps, ethanol structure was disrupted so water could get access. Teng et al.[13,52] observed that on growth pyramids, terrace width decreased with increasing supersaturation. Step width variation with r, i.e., faster growth of the spiral steps with shorter terrace spacing has also been reported.[21,23,53] Recent MD simulations[54] of water−alcohol mixtures showed that the larger ethanol molecules could displace adsorbed water layers on terraces between steps but that at steps, the water remains. There was also a clear effect of terrace length between steps. Thus, the stability of water at the steps suggests that dehydration, as well as attachment and detachment are also influenced by the width of the terraces between the steps.

CONCLUSIONS

Insight into the different growth behavior at the obtuse and acute step edges on calcite was obtained during (i) experiments of calcite step growth under strictly controlled solution conditions with variable saturation index, SI (0.6, 0.8, and 1) and Ca^{2+}:CO_3^{2-} activity ratios, r (0.1, 1, 10, 25, and 50) and (ii) by application and parameter fitting with four different process based growth models. The results provide information for deriving rates of attachment and detachment for each structurally distinct calcite step. We then used the data in (iii) a structural analysis of the atomic configurations at the acute and obtuse steps.

The step velocity data show no discernible change in the conditions for the maximum growth velocity, V_{max}, with SI. Our results do show that obtuse step edges reach a higher V_{max} than acute steps and that the acute step grows faster than the obtuse, at low Ca^{2+}: CO_3^{2-} activity ratios, whereas the obtuse step advances faster at high activity ratios. This implies that not only is the step growth rate controlled by r and SI but also by a modifying factor that is different for each step type. Excess Ca^{2+} accelerates the obtuse step velocity, and excess CO_3^{2-} accelerates the growth rate for the acute step. These observations fit with the atomic structures at the calcite steps as well as parameters for attachment and detachment frequencies derived using step growth rate models. Assuming that termination of the bulk structure does not drastically alter the atomic structures of the steps, we can use that as information for a rough interpretation of attachment affinity. In the {10.4} plane, each carbonate and each calcium ion are coordinated through oxygen in the same way, but the orientation alternates along the step edge. At corners, i.e., a kink site or the exposed corner, every other attachment site has a different orientation, and one of these allows a higher degree of attachment for the adsorbing ion than the others. This understanding, in combination with knowledge about dehydration frequencies, allows us to conclude that Ca^{2+} dehydration determines obtuse step growth rate and CO_3^{2-} incorporation and deprotonation, influenced by atomic configuration in the sites, determines acute step growth.

Our data set is the most extensive and complete that has been collected to date, but none of the currently available growth models are able to describe all our calcite step growth data at nonstoichiometric conditions and they break down for conditions where SI = 1 and Ca^{2+}:$CO_3^{2-} \approx 1$ activity ratios. We suggest that separating the influence of the solution parameters

and the various processes that are involved in controlling growth might lead to more effective predictive models. Fractions of growth sites and atomic structure are important parameters to consider along with solution composition, ion activity ratio, pH, and saturation index.

ASSOCIATED CONTENT

$\mathbf{S}$ Supporting Information

The Supporting Information is available free of charge on the ACS Publications website at DOI: 10.1021/acs.cgd.5b01792.

Detailed information on the modeling of the experimental solution composition, influence of growth site fraction on step rates and parameter values and estimated errors from the fitting procedures (PDF)

AUTHOR INFORMATION

Corresponding Author
*Address: Nano-Science Center Department of Chemistry University of Copenhagen Universitetsparken 5 C-wing, Building B. 2100 Copenhagen E, Denmark. E-mail: kks@nano.ku.dk.

Notes
The authors declare no competing financial interest.

ACKNOWLEDGMENTS

REFERENCES

(1) Mackenzie, F. T.; Andersson, A. *Geochem. Perspect.* **2012**, *1* (2), 3.
(2) Nancollas, G. H.; Reddy, M. M. *J. Colloid Interface Sci.* **1971**, *37* (4), 824−830.
(3) Morse, J. W. *Am. J. Sci.* **1978**, *278* (3), 344−353.
(4) House, W. A. *J. Chem. Soc., Faraday Trans. 1* **1981**, *77* (2), 341−359.
(5) Nielsen, A. E. In *Treatise on Analytical Chemistry*; Kolthoff, I. M., Elving, P. J., Eds.; Wiley: New York, 1983; pp 269−374.
(6) Pokrovsky, O. S.; Schott, J. *Environ. Sci. Technol.* **2002**, *36* (3), 426−432.
(7) Stipp, S. L. S.; Eggleston, C. M.; Nielsen, B. S. *Geochim. Cosmochim. Acta* **1994**, *58* (14), 3023−3033.
(8) Stipp, S. L. S. *Geochim. Cosmochim. Acta* **1999**, *63* (19−20), 3121−3131.
(9) Kristensen, R.; Stipp, S. L. S.; Refson, K. *J. Chem. Phys.* **2004**, *121* (17), 8511−8523.
(10) Hillner, P. E.; Gratz, A. J.; Manne, S.; Hansma, P. K. *Geology* **1992**, *20* (4), 359−362.
(11) Hillner, P. E.; Manne, S.; Gratz, A. J.; Hansma, P. K. *Ultramicroscopy* **1992**, *42-44*, 1387−1393.
(12) Gratz, A. J.; Hillner, P. E. *J. Cryst. Growth* **1993**, *129* (3−4), 789−793.
(13) Teng, H. H.; Dove, P. M.; De Yoreo, J. J. *Geochim. Cosmochim. Acta* **2000**, *64* (13), 2255−2266.

(14) Lasaga, A. C.; Kirkpatrick, R. J. *Kinetics of Geochemical Processes*; Lasaga, A. C., Kirkpatrick, R. J., Series Eds.; Reviews in Mineralogy and Geochemistry; Mineralogical Society of America: Chantilly, VA, 1981; Vol. 8.

(15) Putnis, A. *Introduction to Mineral Sciences*; Cambridge University Press: Cambridge, U.K., 1992.

(16) Teng, H. H.; Dove, P. M.; DeYoreo, J. J. *Geochim. Cosmochim. Acta* **1999**, *63* (17), 2507−2512.

(17) Bracco, J. N.; Grantham, M. C.; Stack, A. G. *Cryst. Growth Des.* **2012**, *12* (7), 3540−3548.

(18) Shiraki, R.; Rock, P.; Casey, W. *Aquat. Geochem.* **2000**, *6* (1), 87−108.

(19) Ruiz-Agudo, E.; Putnis, C. V.; Rodriguez-Navarro, C.; Putnis, A. *Geochim. Cosmochim. Acta* **2011**, *75* (1), 284−296.

(20) Hong, M.; Teng, H. H. *Geochim. Cosmochim. Acta* **2014**, *141* (0), 228−239.

(21) Ruiz-Agudo, E.; Kowacz, M.; Putnis, C. V.; Putnis, A. *Geochim. Cosmochim. Acta* **2010**, *74* (4), 1256−1267.

(22) Nehrke, G.; Reichart, G. J.; Van Cappellen, P.; Meile, C.; Bijma, J. *Geochim. Cosmochim. Acta* **2007**, *71* (9), 2240−2249.

(23) Larsen, K.; Bechgaard, K.; Stipp, S. L. S. *Geochim. Cosmochim. Acta* **2010**, *74* (7), 2099−2109.

(24) Stack, A. G.; Grantham, M. C. *Cryst. Growth Des.* **2010**, *10* (3), 1409−1413.

(25) Wolthers, M.; Di Tommaso, D.; Du, Z.; de Leeuw, N. H. *CrystEngComm* **2013**, *15* (27), 5506−5514.

(26) Zhang, J. W.; Nancollas, G. H. *J. Colloid Interface Sci.* **1998**, *200* (1), 131−145.

(27) Wolthers, M.; Nehrke, G.; Gustafsson, J. P.; Van Cappellen, P. *Geochim. Cosmochim. Acta* **2012**, *77* (0), 121−134.

(28) Hellevang, H.; Miri, R.; Haile, B. G. *Cryst. Growth Des.* **2014**, *14* (12), 6451−6458.

(29) Nielsen, A. E.; Toft, J. M. *J. Cryst. Growth* **1984**, *67* (2), 278−288.

(30) Van Cappellen, P.; Charlet, L.; Stumm, W.; Wersin, P. *Geochim. Cosmochim. Acta* **1993**, *57* (15), 3505−3518.

(31) Pokrovsky, O. S.; Schott, J. *Geochim. Cosmochim. Acta* **1999**, *63* (6), 881−897.

(32) Pokrovsky, O. S.; Mielczarski, J. A.; Barres, O.; Schott, J. *Langmuir* **2000**, *16* (6), 2677−2688.

(33) Wolthers, M.; Charlet, L.; Van Cappellen, P. *Am. J. Sci.* **2008**, *308* (8), 905−941.

(34) Cabrera, N.; Vermilyea, D. A.; *The growth of crystals from solution*; In Growth and Perfection of Crystals: Proceedings of an International Conference on Crystal Growth. Doremus, R. H., Roberts, B. W., Turnbull, D. Eds.; John Wiley & Sons, Inc.: Cooperstown, New York, August 27−29, 1958.

(35) Andersson, M. P.; Rodriguez-Blanco, J. D.; Stipp, S. L. S. *Geochim. Cosmochim. Acta* **2016**, *176*, 198−205.

(36) Sand, K. K.; Pedersen, C. S.; Sjöberg, S.; Nielsen, J. W.; Makovicky, E.; Stipp, S. L. S. *Cryst. Growth Des.* **2014**, *14* (11), 5486−5494.

(37) Christoffersen, J.; Christoffersen, M. R. *J. Cryst. Growth* **1990**, *100* (1−2), 203−211.

(38) Stipp, S. L.; Hochella, M. F. *Geochim. Cosmochim. Acta* **1991**, *55* (6), 1723−1736.

(39) Parkhurst, D. L.; Appelo, C. A. J. *User's Guide to PHREEQC (Version 2) - A Computer Program for Speciation, Batch-Reaction, One-Dimensional Transport, and Inverse Geochemical Calculations*; U.S. Geological Survey Water-Resources Investigations, 1999; p 312.

(40) Plummer, L. N.; Busenberg, E. *Geochim. Cosmochim. Acta* **1982**, *46* (6), 1011−1040.

(41) Hiemstra, T.; Van Riemsdijk, W. H. *J. Colloid Interface Sci.* **1996**, *179* (2), 488−508.

(42) Hiemstra, T.; Venema, P.; Riemsdijk, W. H. V. *J. Colloid Interface Sci.* **1996**, *184* (2), 680−692.

(43) Fenter, P.; Geissbuhler, P.; DiMasi, E.; Srajer, G.; Sorensen, L. B.; Sturchio, N. C. *Geochim. Cosmochim. Acta* **2000**, *64* (7), 1221−1228.

(44) Coleman, T.; Li, Y. *SIAM J. Optim.* **1996**, *6* (2), 418−445.

(45) Storn, R.; Price, K. *J. Glob. Optim.* **1997**, *11* (4), 341−359.

(46) Wolthers, M.; Di Tommaso, D.; Du, Z.; de Leeuw, N. H. *Phys. Chem. Chem. Phys.* **2012**, *14* (43), 15145−15157.

(47) Spagnoli, D.; Kerisit, S.; Parker, S. C. *J. Cryst. Growth* **2006**, *294* (1), 103−110.

(48) van der Weijden, C. H.; van der Weijden, R. D. *J. Cryst. Growth* 5, **2014** *394* (0), 137−144.10.1016/j.jcrysgro.2014.02.042

(49) Sillen, L. G. *Acta Chem. Scand.* **1961**, *15*, 1981−1992.

(50) De Yoreo, J. J.; Gilbert, P. U. P. A.; Sommerdijk, N. A. J. M.; Penn, R. L.; Whitelam, S.; Joester, D.; Zhang, H.; Rimer, J. D.; Navrotsky, A.; Banfield, J. F.; Wallace, A. F.; Michel, F. M.; Meldrum, F. C.; Cölfen, H.; Dove, P. M. *Science* **2015**, *349* (6247), aaa6760.

(51) Sand, K. K.; Yang, M.; Makovicky, E.; Cooke, D. J.; Hassenkam, T.; Bechgaard, K.; Stipp, S. L. S. *Langmuir* **2010**, *26* (19), 15239−15247.

(52) Teng, H. H.; Dove, P. M.; Orme, C. A.; De Yoreo, J. J. *Science* **1998**, *282* (5389), 724−727.

(53) Bracco, J. N.; Stack, A. G.; Steefel, C. I. *Environ. Sci. Technol.* **2013**, *47* (13), 7555−7562.

(54) Keller, K. S.; Olsson, M. H. M.; Yang, M.; Stipp, S. L. S. *Langmuir* **2015**, *31* (13), 3847−3853.